Power, Energy and Electrical Engineering
M. Deng (Ed.)

doi:10.3233/ATDE240360

Efficiency Improvement of Class E Capacitive Power Transfer System Using State Feedback Controller

S. Saat [1], A. Alhattami[1], Y. Yusop[1], S H. Husin[1], M. R. Awal[2], A. H. M. Shapri[3]
[1] *Faculty of Technology and Engineering of Electronic and Computer*
Universiti Teknikal Malaysia Melaka (UTeM)
Melaka, Malaysia
[2] *Faculty of Ocean Engineering, Technology, and Informatics*
Universiti Malaysia Terengganu (UMT)
Kuala Nerus, Malaysia
[3] *Faculty of Electronic & Technology*
Universiti Malaysia Perlis (UNIMAP)
Perlis, Malaysia

Abstract. This paper addresses the enhancement of efficiency in Class E Capacitive Power Transfer (CPT) systems by using a state feedback controller. Efficient operation is a critical concern in CPT systems due to their sensitivity to parameter variations, notably changes in coupling capacitance and load conditions. Variations in these parameters can substantially reduce the overall system efficiency. Therefore, this paper aims to develop a state feedback controller that can bolster system efficiency even in the presence of parameter variations. To be specific, this study begins by modelling the Class E CPT system using a combination of Generalized State-Space Averaging (GSSA) and Frequency-Domain Harmonic Analysis (FHA) techniques. Subsequently, a Lyapunov function is employed to devise the state feedback controller. The problem is then formulated using Linear Matrix Inequalities (LMIs) and tackled through the utilization of Yalmip. The efficacy of the proposed solution is validated through simulation work. The simulation results demonstrate that the proposed controller is capable of maintaining the CPT system's output efficiency at a level exceeding 98%, even when subjected to a maximum of 30% variation in load conditions.

Keywords. Capacitive Power Transfer (CPT), State Feedback Controller, LMI, Yalmip

1. Introduction

The genesis of WPT (Wireless Power Transfer) technology was not a hasty endeavour but rather emerged from the intellectual groundwork laid by Heinrich Hertz in 1888 [1]. WPT presents compelling benefits when compared to physical connections, namely, convenience, safety, and simplicity [2]. In the past few years, WPT has witnessed widespread adoption in a multitude of applications, encompassing smartphone chargers

1 Corresponding author, Shakir Saat, Faculty of Electronics and Computer Technology and Engineering, Universiti Teknikal Malaysia Melaka, 76100, Durian Tunggal, Melaka, Malaysia; E-mail: shakir@utem.edu.my

[3], electric vehicle battery chargers (EV) [4], [5], [6], and biomedical devices [7]. Capacitive Power Transfer, commonly denoted as CPT, employs electric fields to facilitate wireless power transfer. In contrast to IPT, which relies on magnetic fields generated by coils, CPT utilizes capacitor plates or electrodes. It harnesses high-frequency electric fields for the conveyance of electric power, affording it notable advantages when compared to IPT: negligible eddy-current loss, relatively lower cost and weight, outstanding misalignment performance [3], and lower EMI [8].

Increasing the transfer distance in capacitive power transfer leads to a decrease in coupling capacitance, requiring an increase in switching frequency to achieve sufficient power levels. However, this increase in switching frequency results in higher switching losses, leading to a decrease in system efficiency. In order to mitigate low coupling capacitances, the utilization of higher-resonance inductors becomes necessary [8]. However, the adoption of such inductors entails increased conduction losses and a consequent reduction in overall system efficiency. Thus, as indicated in [9], research is conducted on compensation networks for both small and large air-gap applications to determine the optimal compensator for designers. According to the authors, LLC resonant network is suitable for small air-gap CPT applications due to its flexible design, while double-sided LCLC and double-sided LC compensation networks are recommended for large air-gap CPT applications as they offer reduced voltage stress. However, compensation network leads us to other issues, such like, complexity, higher cost, and sensitivity to misalignment [10].

Various control methods have been proposed to address load and coupling capacitance variations in capacitive power transfer (CPT) systems. For example, power flow and linear quadratic Gaussian (LQG) control methods have been suggested to address load variations, while quasi-sliding mode control and hybrid control have been proposed to address coupling capacitance variations. For CPT systems that need to consider both coupling capacitance and load variations, adaptive multi-loop control and robust H∞ method using output feedback control are recommended. However, these control strategies have some issues that can lead to inefficient and unreliable operation of CPT systems. For instance, the phase lock loop (PLL) control method may fail to track the resonant frequency of the CPT system under certain conditions [11]. Similarly, the proportional-integral derivative (PID) control method may not be able to handle the nonlinearities and uncertainties of the CPT system [8]. Fuzzy logic control may also suffer from the same issues [8]. To address these issues, a state feedback controller using Lyapunov approach has been propose. This controller can provide robust and efficient control of CPT systems by ensuring stability and convergence of the system.

2. Analysis of Class E CPT System Using GSSA and FHA Approaches

In this section, we initially derive the first harmonic model of the Class-E-based Capacitive Power Transfer (CPT) system through Frequency-Harmonic Analysis (FHA). Subsequently, a linearization process is undertaken at the system's operational point to establish the linear state-space model for the Class-E-based CPT system. The schematic of Class E-based CPT is shown in Figure 1. While the equivalent circuit of the system is illustrated in Figure 2.

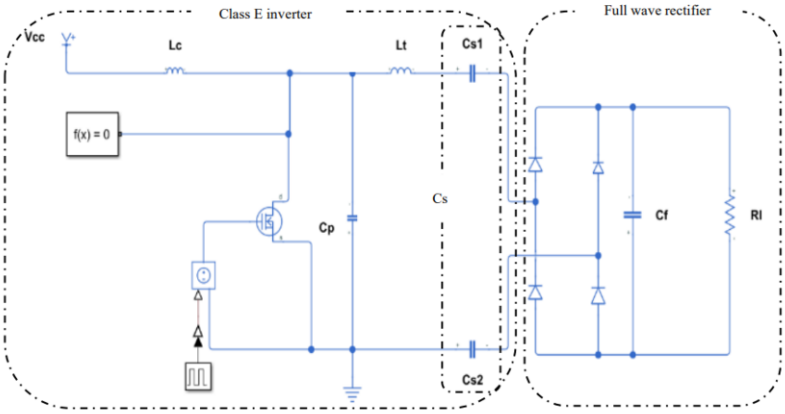

Figure 1. Class-E-based CPT

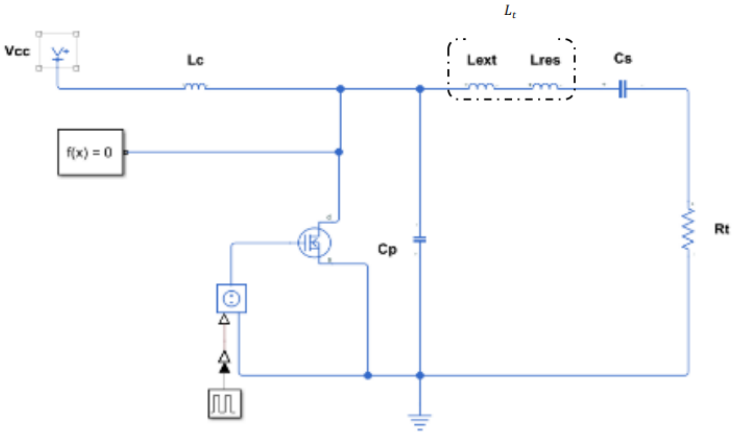

Figure 2. Equivalent circuit of CPT system

The resonant capacitor, Cs, corresponds to the combined equivalent of the series capacitors, Cs1 and Cs2, whereas Re represents the aggregate resistance of the loaded full-wave rectifier, as described in [12]. The calculations provided were comprehensively detailed in [13], [14].

$$C_s = \frac{C_{s1} * C_{s2}}{C_{s1} + C_{s2}} \tag{1}$$

$$R_t = \frac{8 * R_l}{\pi^2} \tag{2}$$

where R_l is the load resistance.

The first harmonic model of CPT is based on the following assumptions [15]:

i. The choke inductance value, Lc, is sufficiently high to provide current with a low ripple factor. This means that the alternating current component of the input current is significantly lower than the direct current component.

The research is funded by Ministry of Higer Education through Fundamental Research Grant Scheme funding (FRGS/1/2022/TK07/UTEM/02/46).

ii. The circuit's quality factor, Q, is high enough to effectively suppress the harmonics of the fundamental frequency.
iii. The MOSFET switch being used is ideal, meaning it has no on-resistance, infinite off resistance, and zero switching time.
iv. In the circuit, all diodes are ideal, meaning they only allow current to pass through in one direction. When the diodes turn on, their forward voltage is zero, and they behave like perfect conductors. On the other hand, when the diodes are off, they effectively block current flow in the reverse direction.
v. The duty cycle, D = 0.5.

According to [16], the calculation that used to obtain the values of components in

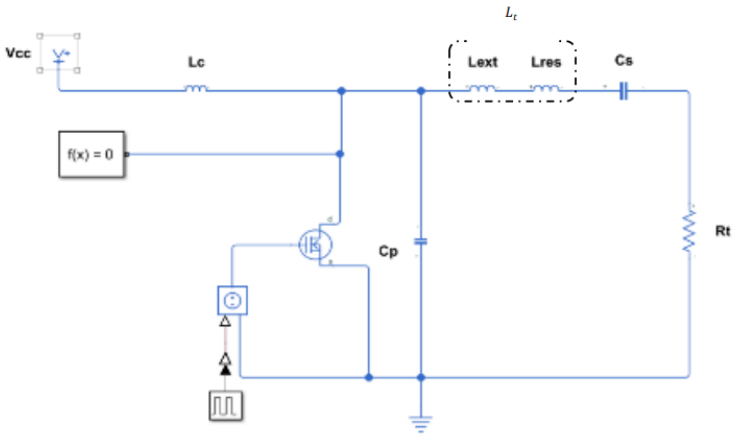

Figure **2.** Equivalent circuit of CPT system is as follows; the output power of the system, Po is calculated using the following equation;

$$P_o = \frac{8V_{cc}}{(\pi^2+4)R_t} \tag{3}$$

The resonant inductance, L_t, was separated into two components, L_{ext} and L_{res}, which were computed using the following:

$$L_t = \mathrm{L_{ext}} + \mathrm{L_{res}} \tag{4}$$

$$\mathrm{L_{ext}} = \frac{1.153\,R_t}{w} \tag{5}$$

$$\mathrm{L_{res}} = \frac{Q\mathrm{R_t}}{w} \tag{6}$$

Where, Q is quality factor, and w is switching frequency. Meanwhile, C_p, is the shunt capacitance, giving as:

$$\mathrm{C_p} = \frac{\mathrm{P_o}}{\pi w {V_{cc}}^2} \tag{7}$$

The resonant capacitance, C_s can obtained by using:

$$C_s = \frac{1}{wQR_t} \tag{8}$$

The chock inductor's minimum value calculated as follow:

$$L_c = 2\left(\frac{\pi^2}{4} + 1\right)\frac{R_t}{f} \tag{9}$$

V_{AB} is the voltage across MOSFET, in our design, the value of V_{AB} is crucial, especially when applied to the first harmonic. Hence it can be obtained using the following equation.

$$V_{AB} = \begin{cases} \frac{I_o}{wC_p}[wt - \frac{3\pi}{2} - \frac{\pi}{2}\cos(wt) - \sin(wt)] & \pi < wt < 2\pi \\ 0 & 0 < wt < \pi \end{cases} \tag{10}$$

3. Modelling of CPT System

By analysing the equivalent circuit in Figure 1 using Kirchhoff's current and voltage laws (KVL, and KCL), the voltage across the Cp, VAB can be written as,

$$\begin{cases} V_{AB} = L_t \frac{di}{dt} + V_{cs} + sgn\,(i)\,V_f \\ i = C_s \frac{dv_{cs}}{dt} \\ |i| = C_f \frac{dv_f}{dt} + \frac{v_f}{R_l} \end{cases} \tag{11}$$

System output voltage, $sgn\,(x)$ is a symbol of function and it is given as,

$$sgn\,(x) = \begin{cases} 1 & x < 0 \\ 0 & x = 0 \\ -1 & x > 0 \end{cases} \tag{12}$$

According to [17], the symbol, $sgn\,(x)$ can be approximated as

$$\begin{cases} sgn\,(i) = \frac{4\,i_s}{\pi i_p}\sin(wt) + \frac{4\,i_c}{\pi i_p}\cos(wt) \\ |i| \approx \frac{2}{\pi} i_p \\ i_p = \sqrt{{i_s}^2 + {i_c}^2} \end{cases} \tag{13}$$

Equation (11) was used to determine the state vectors of the system, namely, i, V_{cs}, and V_f. Despite being an energy-storing element, the shunt capacitor, C_p, was not considered as a state variable as its waveform is non-differentiable and its dynamic behaviour is entirely determined by the energy stored in the series capacitor, C_{cs}, and the resonant inductor, L_t.

Then, using Fourier series expansion, the first harmonic of the series current i, which flows through L_t and C_s, and the voltage V_{cs} applied to capacitor C_s can be expressed according to the FHA.

$$\begin{cases} i = i_s \sin wt + i_c \cos wt \\ v_{cs} = v_s \sin wt + v_c \cos wt \end{cases} \tag{14}$$

By differentiating both side of (14), we have

$$\begin{cases} \frac{di}{dt} = \left(\frac{di_s}{dt} - wi_c\right)\sin(wt) + \left(\frac{di_c}{dt} + wi_s\right)\cos(wt) \\ \frac{di_{vc}}{dt} = \left(\frac{dv_s}{dt} - wv_c\right)\sin(wt) + \left(\frac{dv_c}{dt} + wv_s\right)\cos(wt) \end{cases} \tag{15}$$

According to FHA, the first harmonic of the voltage V_{AB} is described by:

$$V_{AB} = a_1 \sin(wt) + b_1 \cos(wt) \tag{16}$$

where a_1, and $b_1$are,

$$\begin{cases} a_1 = \frac{1}{\pi}\int_{\pi}^{2\pi} v_{AB} \sin(wt)\, d(wt) = -\frac{\pi V_{cc}}{2} \\ b_1 = \frac{1}{\pi}\int_{\pi}^{2\pi} v_{AB} \cos(wt)\, d(wt) = \frac{(8-\pi^2)V_{cc}}{4} \end{cases} \tag{17}$$

Furthermore, substituting (13), (14), (15), (16), and (17) into (11), and by setting the coefficients of the DC, sine, and cosine terms equal to each other, one can derive the state-space equation as follows:

$$\begin{cases} L_t \frac{di_s}{dt} = L_t w i_c - v_s - \frac{4i_s}{\pi i_p} v_f - \frac{\pi V_{cc}}{2} \\ L_t \frac{di_c}{dt} = -L_t w i_s - v_c - \frac{4i_c}{\pi i_p} v_f + \frac{(8-\pi^2)V_{cc}}{4} \\ C_s \frac{dv_s}{dt} = i_s + C_s w v_c \\ C_s \frac{dv_c}{dt} = i_c - C_s w v_s \\ C_f \frac{dv_f}{dt} = \frac{2}{\pi} i_p - \frac{v_f}{R_l} \end{cases} \tag{18}$$

In steady state, the state vector does not vary with respect to time. This means that the partial differential in equation (22) of the large signal model with respect to time is equal to zero. As a result, where I_p and V_f are the steady-state values of i_p and v_f respectively. Hence,

$$I_p = \frac{\pi V_f}{2R_l} \tag{19}$$

Note 1 : let us donate the steady state of $x = [i_c\ i_s\ v_c\ v_s\ v_f]$ and w, as $x_{ss} = [I_c\ I_s\ V_c\ V_s\ V_f]$ and W respectively. Substitute (19) into (18) gives:

$$\begin{cases} \frac{dI_s}{dt} = w(I_c) - \frac{1}{L_t}(V_s) - \frac{8R_l}{\pi^2 L_t}(I_s) - \frac{\pi V_{cc}}{2L_t} \\ \frac{dI_c}{dt} = -w(I_s) - \frac{1}{L_t}(V_c) - \frac{8R_l}{\pi^2 L_t}(I_c) + \frac{(8-\pi^2)V_{cc}}{4L_t} \\ \frac{dV_s}{dt} = \frac{1}{C_s}(I_s) + w(V_c) \\ \frac{dV_c}{dt} = \frac{1}{C_s}(I_c) - w(V_s) \end{cases} \tag{20}$$

From (20), the steady state model of the system is as follows:

$$A_{ss} = \begin{bmatrix} -\frac{8R_l}{\pi^2 L_t} & w & -\frac{1}{L_t} & 0 \\ -w & -\frac{8R_l}{\pi^2 L_t} & 0 & -\frac{1}{L_t} \\ \frac{1}{C_s} & 0 & 0 & w \\ 0 & \frac{1}{C_s} & -w & 0 \end{bmatrix}, \quad B_{ss} = \begin{bmatrix} -\frac{\pi V_{cc}}{2L_t} \\ \frac{(8-\pi^2)V_{cc}}{4L_t} \\ 0 \\ 0 \end{bmatrix}$$

The system in (18) is a nonlinear system, it must be linearized at its equilibrium points. The equilibrium points can be determined by setting equation (18) to zero and solving for the state variables as follows;

$$0 = A * X_e + B * V_{cc} \rightarrow X_e = A^{-1} * B * V_{cc}$$

The linear model is obtained by applying the Taylor series linearization method to the nonlinear model. The resulting state space representation is then written as:

$$\begin{cases} \dot{\hat{x}} = A\hat{x} + B\hat{u} \\ \hat{y} = C\hat{x} \end{cases} \tag{21}$$

where A, B, and C are the state, input, and output matrices respectively. While $\hat{x}$ is the state vector, $\hat{u}$ is the input vector and $\hat{y}$ is the output vector.

$$\hat{x} = [\hat{\imath}_s, \quad \hat{\imath}_c, \quad \hat{v}_s, \quad \hat{v}_c, \quad \hat{v}_f]^t$$
$$\hat{u} = \hat{w}$$
$$\hat{y} = \hat{v}_f$$

So, the A, B, and C matrices can now be written as follows:

$$A = \begin{bmatrix} -\frac{4{I_c}^2 V_f}{\pi L_t {I_p}^3} & w_0 + \frac{4I_c I_s V_f}{\pi L_t {I_p}^3} & -\frac{1}{L} & 0 & -\frac{4I_s}{\pi L_t I_p} \\ \frac{4I_c I_s V_f}{\pi L_t {I_p}^3} - w_0 & -\frac{4{I_c}^2 V_f}{\pi L_t {I_p}^3} & 0 & -\frac{1}{L} & -\frac{4I_c}{\pi L_t I_p} \\ \frac{1}{C_s} & 0 & 0 & w_0 & 0 \\ 0 & \frac{1}{C_s} & -w_0 & 0 & 0 \\ \frac{2I_s}{\pi C_p I_p} & \frac{2I_c}{\pi C_p I_p} & 0 & 0 & \frac{1}{R_l C_f} \end{bmatrix}$$

$$B = \begin{bmatrix} I_c \\ -I_s \\ V_c \\ -V_s \\ 0 \end{bmatrix} \tag{22}$$

$$C = [0 \quad 0 \quad 0 \quad 0 \quad 1]$$

The model (22) will be used in this work and before it can be applied here the model given in (22) must be validated first and this will be discussed in the next section.

4. Model Validation

The MATLAB software is used validate the performance of the CPT system under different loads. As previously discussed in section II, the parameters of the system were determined through analysis and assumptions made about the Class E inverter. The values for the input voltage, Vcc = 24 V, series resonant capacitance, Cs = 122.72 pF, resonant inductance, Lt = 54.57 µH, at switching frequency f = 2 MHz, output capacitance, Cf= 20 µF, choke inductance, Lc = 112.48 µH, and Quality factor, Q = 20. According to the simulation results shown in Fig. 3, both the drain voltage and switching voltage waveforms were obtained and it was observed that the zero-voltage-switching (ZVS) is perfectly achieved.

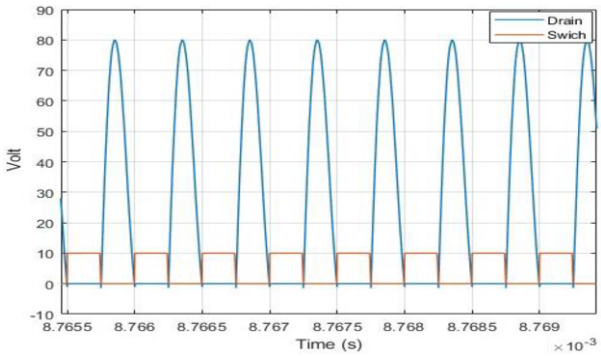

Figure 3. Drain vs switch voltage

The output voltage of the CPT system is illustrated in Fig. 4 with R_l = 40 ohm. It is obvious from the figure that the output voltage of the model (22) is perfectly aligned with the simulation circuit. This certify that the model given in (22) can be used in this work for controller design purpose. Meanwhile, to study the effect of the load variation to the CPT system, R_l is then varied to 60 ohms at t = 6 ms as shown in Fig. 5. The solid line shows the simulation result, whereas the dashed markers show the behavioural of the model outcome. The output voltage increased from 14.42 V to 17.96 V when the load varied from 40 Ohms to 60 Ohms. These changes will affect the overall performance of the CPT system and justify the need to have the controller to control and stabilize the system despite load variation. The state feedback controller is chosen here, and it is discussed in the next text.

Remark 1: We can elucidate from Fig 4 and Fig 5 that the modelling is identical with the system which is critical to design a control system

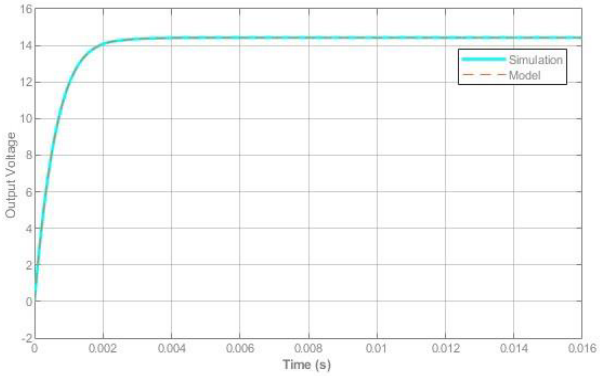

Figure 4. Output voltage for CPT system.

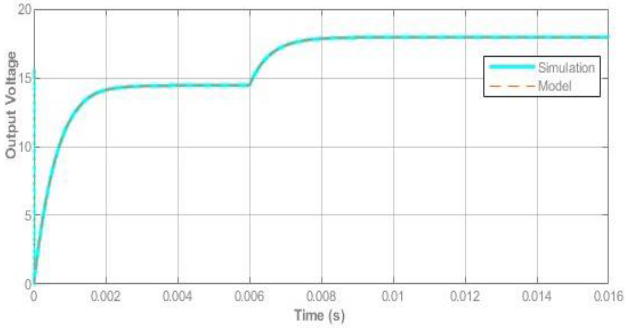

Figure 5. Output voltage for CPT system with load variation.

5. State Feedback Controller Design

In Class E CPT systems, efficient energy transfer is paramount yet challenging due to susceptibilities to parameter variations such as load conditions and coupling capacitances. These variations can significantly impede the system's efficiency. To counteract this, a state feedback controller is introduced in this work. The generic form of a state feedback controller is $u = Kx$, where u is the control input, x is the state vector, and K is the gain matrix. The state feedback controller directly manipulates the system's states through real-time measurements, thereby ensuring robust performance. The primary purpose of employing a state feedback controller in CPT systems is to maintain high efficiency, even in the face of varying conditions. By continually adjusting the system in real-time, the state feedback controller aims to sustain output efficiency levels above a specified target, such as 80%, thus fulfilling the operational demands without compromising on performance.

Let consider the following system.

$$\dot{X} = Ax + Bu \tag{22}$$

$$y = Cx \tag{23}$$

The state feedback controller is then proposed as

$$u = -Kx \tag{24}$$

where x is the state vector, u is the control input, A is a system matrix, B is an input matrix, C is an output matrix and K is the control gain matrix. Here, A, B and C matrices are as the CPT model developed in section 错误!未找到引用源。. However, it is important to note that only A matrix is affected by the load variation.

Theorem1: The system (22) is asymptotically stable via state feedback controller (24) if and only if there exist a symmetrical matrix P and the conditions are satisfied.

P>0

$$[x]^T \begin{bmatrix} A & B \\ B^T & C \end{bmatrix} [x] \leq 0 \tag{25}$$

where,

$$A = A^T P + PA$$

$$B = -(PBK + K^T B^T P)$$

$$C = 0$$

Let,

$$L = PBK$$

So, the controller gain, K can be found as

$$K = L(PB)^{-1}$$

Proof:

The Lyapunov function is chosen as.

$$V = x^T P x$$

where P is the positive definite Lyapunov matrix and V must satisfy the following condition to ensure stability of the system with.

$$V(x) > 0$$

$$\frac{dv}{dx} \leq 0$$

$$\frac{d(x^T P x)}{dx} = \dot{x}^T P x + x^T P \dot{x} \leq 0$$

$$\frac{dv}{dx} = (Ax + Bu)^T P x + x^T P (Ax + Bu) \leq 0$$

$$= (A^T x^T + B^T u^T) P x + x^T P (Ax + Bu) \leq 0$$

$$= (A^T x^T + B^T(-Kx)^T)Px + x^T P(Ax + B(-Kx)) \leq 0$$
$$= (A^T x^T Px - B^T K^T x^T Px + x^T PAx - x^T BPKx) \leq 0$$
$$= x^T (A^T P + AP - K^T B^T P - PBK)x \leq 0$$

From this, you can infer that A, and B value are as follow:

$$A = (A^T P + PA)$$
$$B = -(PBK + K^T B^T P)$$

Then by using Schur complement, we arrive at

$$\begin{bmatrix} X \\ \dot{X} \end{bmatrix}^T \begin{bmatrix} A^T P + PA & -(PBK + K^T B^T P) \\ -(PBK + K^T B^T P)^T & 0 \end{bmatrix} \begin{bmatrix} X \\ \dot{X} \end{bmatrix} \leq 0$$

The proof ends.

6. Simulation Results

In this section the result of the controller is discussed in detail. This result is based on the parameter simulation as in Table 1. The MATLAB software is used to simulate the SFC. Yalmip is utilized to obtain the feasible solution to the formulated solution.

Table 1. CPT system parameters

Symbol	Parameter	Value
V_{cc}	DC Supply Voltage	24 V
C_{s1}, C_{s2}	Coupling Capacitance	3.4 nF
C_s	Equivalent Coupling Capacitance	1.7 nF
R_L	Load Resistor	40 Ω
f	Switching Frequency	1 MHz
C_f	DC Output Capacitor	54 μF
V_{out}	Desired System Output Voltage	14.6 V
C_p	Shunt Capacitor	1.64 nF
L_t	Series Inductor	18.17 μF

The result of the CPT system output voltage with SFC is shown in Figure 6, the load is varied at two different point where the first one is made at t=0.025s and the second one is at t= 0.055s. At the first point, the load is reduced by 30% from its nominal value meanwhile at the second point, the load is varied to +30% from its nominal value. The load nominal value for this Class E CPT system is 40 ohms. It is obvious that the proposed SFC able to stabilize the system well despite the variation in load. Here, the controller gain, K is obtained based on theorem 1 as; K1=1.0e+05*[2.9757], K2= 1.0e+05*[-0.0010], K3=1.0e+05*[0.0002], K4=1.0e+05*[-0.0042] and K5=1.0e+05*[-0.1794]

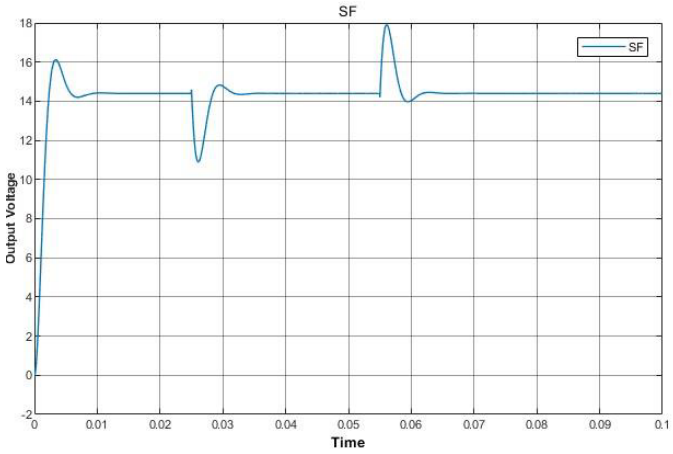

Figure 6. Output voltage for CPT system with control and load variation

It is important to note as well that the efficiency of the Class E CPT system with SFC is 98.93%. This is above the targeted one which is 80%.

7. Conclusion

This paper presents a Capacitive Power Transfer (CPT) system using a Class E inverter and dynamically modeled via the Generalized State-Space Averaging (GSSA) technique. MATLAB was employed for both validating and simulating the CPT model. State Feedback (SF) controllers in this setup were formulated to stabilize the output voltage amid load fluctuations. Developed using Lyapunov principles, the SF controllers were tested against two distinct disturbances to verify their robustness. Simulation outcomes revealed that these controllers enhanced the CPT system's response to load changes. Moreover, the Lyapunov-based design resulted in SF controllers that yielded consistent output voltages, irrespective of variations in the load. The future work lies on the robust H infinity performance of the CPT system.

Acknowledgment

Authors would like to thank the Ministry of Higer Education for providing a Fundamental Research Grant Scheme funding (FRGS/1/2022/TK07/UTEM/02/46).

Authors would like to thank Universiti Teknikal Malaysia Melaka (UTeM) as well for all the supports.

References

[1] T. S. Chandrasekar Rao and K. Geetha, "Categories, standards and recent trends in wireless power transfer: A survey," Indian J. Sci. Technol., vol. 9, no. 20, May 2016, doi: 10.17485/ijst/2016/v9i20/91041.
[2] G. Ombach, "Design and safety considerations of interoperable wireless charging system for automotive," 2014 9th Int. Conf. Ecol. Veh. Renew. Energies, EVER 2014, 2014, doi: 10.1109/EVER.2014.6844157.
[3] F. Lu, H. Zhang, and C. Mi, "A review on the recent development of capacitive wireless power transfer technology," Energies, vol. 10, no. 11, 2017, doi: 10.3390/en10111752.
[4] M. Salem, A. Jusoh, N. Nik Idris, and I. Alhamrouni, "A review of an inductive power transfer system for EV battery charger," Eur. J. Sci. Res., vol. 107, no. 1, pp. 42–56, 2013.
[5] C. Bhuvaneswari and R. S. R. Babu, "A review on LLC Resonant Converter," 2016 Int. Conf. Comput. Power, Energy, Inf. Commun. ICCPEIC 2016, pp. 620–623, 2016, doi: 10.1109/ICCPEIC.2016.7557268.
[6] Y. Geng, Z. Yang, and F. Lin, "Design and Control for Catenary Charged Light Rail Vehicle Based on Wireless Power Transfer and Hybrid Energy Storage System," IEEE Trans. Power Electron., vol. 35, no. 8, pp. 7894–7903, 2020, doi: 10.1109/TPEL.2020.2966218.
[7] S. Kim, J. S. Ho, and A. S. Y. Poon, "Wireless power transfer to miniature implants: transmitter optimization," IEEE Trans. Antennas Propag., vol. 60, no. 10, pp. 4838–4845, 2012, doi: 10.1109/TAP.2012.2207341.
[8] M. Z. Erel, K. C. Bayindir, M. T. Aydemir, S. K. Chaudhary, and J. M. Guerrero, "A Comprehensive Review on Wireless Capacitive Power Transfer Technology: Fundamentals and Applications," IEEE Access, vol. 10, pp. 3116–3143, 2022, doi: 10.1109/ACCESS.2021.3139761.
[9] D. Rozario, S. Member, N. A. Azeez, S. S. Williamson, and S. Member, "Comprehensive Review and Comparative Analysis of Compensation Networks for Capacitive Power Transfer Systems," 2000.
[10] M. Al-saadi, E. A. Hussien, S. Ahmed, and A. Craciunescu, "Comparative Study of Compensation Circuit Topologies in 6. 6kW Capacitive Power Transfer System," no. September 2020, 2019.
[11] Z. Wang, Y. Zhang, X. He, B. Luo, and R. Mai, "Research and Application of Capacitive Power Transfer System: A Review," Electron., vol. 11, no. 7, 2022, doi: 10.3390/electronics11071158.
[12] T. M. Mostafa, D. Bui, A. Muharam, R. Hattori, and A. P. Hu, "A Capacitive Power Transfer System with a CL Network for Improved System Performance," 2018 IEEE Wirel. Power Transf. Conf. WPTC 2018, pp. 1–4, 2019, doi: 10.1109/WPT.2018.8639497.
[13] S. Aldhaher, D. C. Yates, and P. D. Mitcheson, "Modeling and Analysis of Class EF and Class E/F Inverters with Series-Tuned Resonant Networks," IEEE Trans. Power Electron., vol. 31, no. 5, pp. 3415–3430, 2016, doi: 10.1109/TPEL.2015.2460997.
[14] M. Yousefi, Z. D. Koozehkanani, J. Sobhi, H. Jangi, and N. Nasirezadeh, "Efficiency analysis of low power class-E power amplifier," Mod. Appl. Sci., vol. 8, no. 5, pp. 19–29, 2014, doi: 10.5539/mas.v8n5p19.
[15] N. O. Sokal and A. D. Sokal, "Class of High-Efficiency Tuned Switching Power Amplifiers," IEEE J. Solid-State Circuits, vol. 10, pp. 168–76, 1975.
[16] T. Suetsugu and M. K. Kazimierczuk, "Analysis and design of class E amplifier with shunt capacitance composed of nonlinear and linear capacitances," IEEE Trans. Circuits Syst. I Regul. Pap., vol. 51, no. 7, pp. 1261–1268, 2004, doi: 10.1109/TCSI.2004.830695.
[17] P. Wang, C. Liu, and L. Guo, "Modeling and simulation of full-bridge series resonant converter based on generalized state space averaging," Appl. Mech. Mater., vol. 347–350, pp. 1828–1832, 2013, doi: 10.4028/www.scientific.net/AMM.347-350.1828.